Electronic Supplementary Information

Fine-tuning the magnetocaloric effect and SMMs behaviors of coplanar RE_4 complexes by β-diketonate coligands

Hong-Ling Gao,[a,b*] Ni-Ni Wang,[a] Wen-Min Wang,[a] Hai-Yun Shen,[a] Xiao-Pu Zhou,[a] Yi-Xin Chang,[a] Ru-Xia Zhang,[a] Jian-Zhong Cui[a*]

[a]*Department of Chemistry, Tianjin University, Tianjin 300354, People's Republic of China.*

[b]*Key Laboratory of Advanced Energy Materials Chemistry (Ministry of Education), Nankai University, Tianjin 300071, China.*

*Corresponding author. *E-mail address*: cuijianzhong@tju.edu.cn; ghl@tju.edu.cn.

List of Contents

Section S1 Supplementary Experimental Section

Synthesis of 5-[(3-methyl-2-thiopheneformaldehyde)-amino]-8-hydroxylquinoline (HL)

5-amino-8-hydroxylquinoline. The synthesis of 5-amino-8-hydroxyquinoline was optimized compared to the method reported previously in the literature.[1] A mixture of 5-nitryl-8-hydroxylquinoline (4.75 g, 0.025 mol) and 5 % Pd/C (0.0625 g), which was used as catalyst, in a 1.3 % ratio in absolute isopropanol was heated to 70 °C, and then 5 mL of 80 % hydrazine hydrate was dropped into the mixture over 30 minutes. It was heated to 92 °C and refluxed for 4 h. Finally, the solvent was removed, and dichloromethane was used to wash the grass green solid product (yield 2.7 g, 67.5%). Elemental analysis (%): Calcd for $C_9H_8ON_2$ (fw = 160.42): C 67.32, H 5.00, N 17.50. Found: C 67.28, H 4.97, N 17.82. IR (KBr, cm^{-1}): 3344 (s), 1688 (s), 1626 (s), 1489 (s), 1346 (s), 915 (s), 746 (m).

5-[(3-methyl-2-thiopheneformaldehyde)-amino]-8-hydroxylquinoline (HL)

5-Amino-8-hydroxylquinoline (0.8 g, 5 mmol) was dissolved in 10 mL ethanol at 55 °C, and 0.57 mL of 3-methyl-2-thiopheneformaldehyde was added, and 3–4 drops of formic acid was dropped into the mixture as a catalyst. After that, the mixture was heated for 4 h at 75 °C. The product was isolated from the mixture and it was purified by recrystallization from a mixed solvent of ethanol and acetone (3/1, v/v). The purified product was obtained as a green solid (yield 1.12 g, 72.25 %). Elemental analysis (%): Calcd for $C_{15}H_{12}N_2OS$ (fw = 268.34): C 67.08, H 4.51, N, 10.44. Found C 67.23, H 4.59, N 10.57. IR (KBr, cm^{-1}): 3284 (m), 3049 (w), 1658 (w), 1593 (s), 1503 (s), 1471 (m), 1406 (s), 1375 (m), 1276 (s), 1226 (m), 1188 (s), 1157 (m), 1050 (m), 823 (w), 785 (m), 710 (s), 670 (m), 579 (w), 494 (w), 418 (w).

[1] A. Lilienkampf, J. L. Mao, B. J. Wan, Y. H. Wang, S. G. Franzblau, A. P. Kozikowski, *J. Med. Chem.*, 2009, **52**, 2109.

Section S2 Thermogravimetric Analysis and Powder X-ray Diffraction

To confirm the thermal stability of complexes **1–10**, TGA was performed under air

atmosphere with a heating rate of 10 °C min^{-1} in 30–800 °C (Fig. S2†). The curves of **1**–**7** indicated the thermal stability up to 300 °C, because they were kept for a period of time under ambient conditions resulting in the spontaneous loss of solvent molecules. Then complexes **1**–**7** experience continuous process of weightlessness until the metal organic framework divided in the temperature range of 300–750 °C. What's more, the curves of **8**–**10** are similar to **1**–**7**, crystalline samples keep unchanged in the range of 30–100 °C, after display a main weight loss taking place between 200 and 750 °C, which is related to the release of the organic ligands. Finally, the residue of **1**–**10** is expected to be the corresponding lanthanide oxide RE_2O_3.

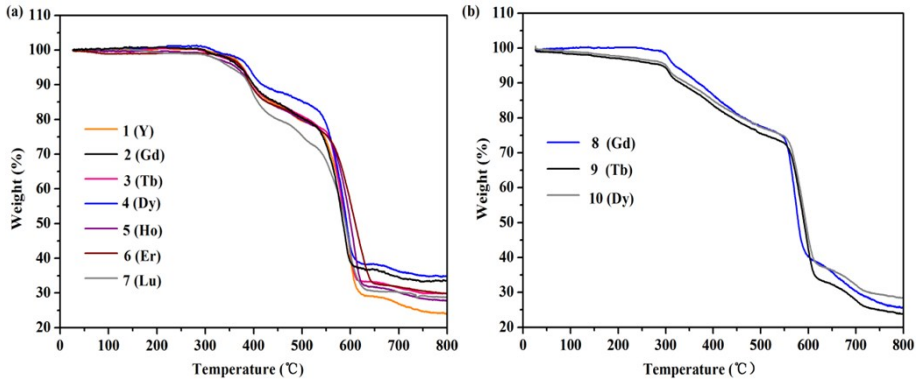

Fig. S2 TGA curves of **1**–**7** and **8**–**10** (a and b) on crystalline samples under the air atmosphere in the temperature range of 30 – 800 ˚C.

In order to verify purity of the crystalline samples, complexes **1**–**10** have been characterized by powder X-ray diffraction (PXRD) at room temperature (Fig. S3†). The experimental patterns of **1**–**10** consistent with the simulated patterns of the single crystal data suggesting that the presence of mainly one crystalline phase.

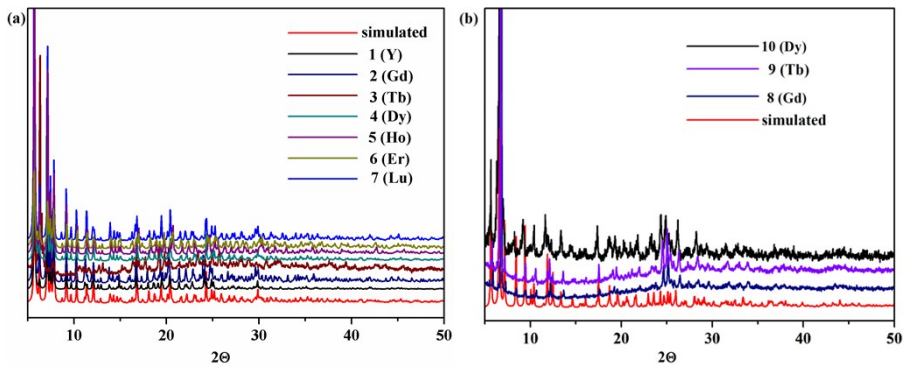

Fig. S3 PXRD patterns for **1–7** (a) and **8–10** (b).

Section S3 UV-Vis Spectra

The UV-vis absorption spectra of HL, $Tb(dbm)_3 \cdot 2H_2O$, $Tb(acac)_3 \cdot 2H_2O$ and complexes **1–10** were measured in CH_2Cl_2 solution (10^{-5} mol L^{-1}) at room temperature (Fig. S4†). For $Tb(dbm)_3 \cdot 2H_2O$, two absorption bonds are observed at ca. 253 and 344.5 nm, while $Tb(acac)_3 \cdot 2H_2O$ displays a single intense absorption band at ca. 284 nm. HL is composed of three absorption bonds at ca. 253, 286, and 378 nm respectively, and the strongest bond at ca. 253 nm may be attributed to $\pi \rightarrow \pi^*$ transition of the aromatic rings. In contrast, complexes **1–7** display three analogous sets of absorption bands at ca. 261, 358, and 421 nm, respectively. The main absorption bond at ca. 261 nm may be contributed to intraligand $\pi \rightarrow \pi^*$ transition of dbm^- coligands and L^- ligands, and the broad low energy band at ca. 421 nm may be ascribed to the extended $n \rightarrow p^*$ transition in Schiff base ligands bound to the RE^{III} cations. However, the absorption spectra of **8–10** show two absorption bands at ca. 255 and 381 nm, the poorer energy transition may be due to the extended $n \rightarrow p^*$ transition in Schiff base ligands bound to the RE^{III} cations. Besides, the absorption bands in **1–10** have a slight red shift relative to the free HL, the absorption peak at 286 nm of HL has disappeared when coordinated with RE^{III} cations, which can be ascribed to the coordination effect between the L^- and RE^{III} cations.

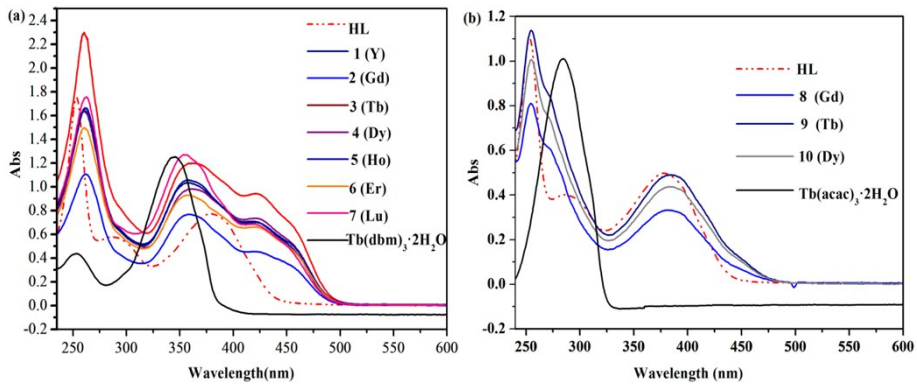

Fig. S4 UV-vis absorption spectra of complexes **1–7** (a) and **8–10** (b) in CH_2Cl_2 solution at room temperature.

Section S4 Supplementary Table S1 – S7

Table S1 The important bond lengths (Å) and angles (°) of complexes **1–10**.

Complexes	The range of RE–O bond lengths / Å	The range of RE–N bond lengths / Å	The distance of RE···RE / Å	The range of O–RE–O bond angles / º	The bond angles of RE–RE–RE / º
1	2.296(5) – 2.414(4)	2.496(6) – 2.538(5)	3.5405(10), 3.8487(10)	66.94(14) – 146.50(14)	61.666(18), 118.334(24)
2	2.328(3) – 2.468(3)	2.540(3) – 2.585(3)	3.6096(3), 3.9199(3)	67.19(9) – 146.85(9)	61.770(6), 118.230(7)
3	2.311(2) – 2.465(2)	2.530(3) – 2.573(3)	3.5889(3), 3.9009(3)	66.79(7) – 147.18(7)	61.558(6), 118.443(6)
4	2.294(5) – 2.448(4)	2.525(6) – 2.550(6)	3.5651(6), 3.8794(5)	66.93(15) – 147.01(15)	61.521(9), 118.479(12)
5	2.282(3) – 2.437(3)	2.506(4) – 2.553(4)	3.5505(4), 3.8619(4)	66.88(11) – 146.60(11)	61.474(9), 118.526(9)
6	2.291(5) – 2.407(4)	2.485(6) – 2.535(5)	3.5319(6), 3.8395(5)	68.64(14) – 146.28(14)	61.50(1), 118.50(12)
7	2.254(2) – 2.383(2)	2.471(3) – 2.518(3)	3.4872(5), 3.7996(3)	66.55(8) – 146.64(7)	61.331(9), 118.669(12)
8	2.300(11) – 2.469(8)	2.549(9) – 2.579(9)	3.6102(8), 3.8852(8)	68.8(3) – 143.9(2)	62.138(16), 117.862(19)
9	2.304(3) – 2.450(3)	2.532(4) – 2.552(4)	3.5916(3), 3.8670(3)	66.84(10) – 146.67(10)	61.948(6), 118.052(7)
10	2.266(12) – 2.429(8)	2.512(10) – 2.538(11)	3.5713(8), 3.8436(8)	68.3(3) – 146.7(3)	61.998(15), 118.002(18)

Table S2 The continuous symmetry measurement value calculated by SHAPE 2.0 for complexes **2** and **8**.

Complex **2**	D_{4d}SAPR	D_{2d}TDD	C_{2v}JBTPR	C_{2v}BTPR	D_{2d}JSD
Gd1	0.965	2.292	2.384	1.843	4.654
Gd2	1.525	1.666	3.234	2.497	4.404

Complex **8**	D_{4d}SAPR	D_{2d}TDD	C_{2v}JBTPR	C_{2v}BTPR	D_{2d}JSD
Gd1	1.313	1.810	2.810	1.976	4.715
Gd2	1.103	2.157	2.791	2.241	4.371

Table S3 The parameters ***C*** and ***θ*** of **2–6** and **8–10** were generated from the best fit by the Curie-Weiss expression.

complexes	**2**-Gd	**3**-Tb	**4**-Dy	**5**-Ho	**6**-Er	**8**-Gd	**9**-Tb	**10**-Dy
C / cm^3 K mol^{-1}	34.04	48.22	55.52	58.48	46.68	32.88	50.35	57.08
θ / K	-1.38	-2.37	-2.32	-8.24	-6.19	-1.44	-4.20	3.37

Table S4 Parameters obtained from the ln (τ) vs. T^{-1} plots using the eq 1 for **4** and **10**.

complex	U_{eff}/ K	τ_0 /s	τ_{QTM} /s	A	m	C	n
4, H_{dc}=0	93.23	3.88E-7	0	0	0	43.68	1.75
10, H_{dc}=0	37.49 (FR)	7.73E-6	--	--	--	--	--
	89.89 (SR)	5.66E-7	1.03	25.42	0	539.65	1.02
4, H_{dc}=1000	109.48	1.22E-8	6.3E-3	0	0	16.11	2.31
10, H_{dc}=1500	116.20	5.18E-8	0	0	0	50.11	2.03

Table S5 The parameters obtained from cole-cole plots using the Debye model for **4** and **10** under zero dc field.

Slow Relaxation (SR) of **4** under zero dc field			
T / K	χ_1	χ_2	α
2.0	0.45061	20.46657	0.56048
2.5	0.4527	17.14349	0.5461
3.0	0.4985	14.43886	0.52434
3.5	0.43178	13.21244	0.53362
4.0	0.4758	11.34914	0.51261
4.5	0.46515	10.44611	0.51053
5.0	0.47638	9.55962	0.5021
5.5	0.48516	8.86239	0.49548
6.0	0.48023	8.33256	0.49462
6.5	0.53813	7.59065	0.47152
7.0	0.54586	7.12097	0.46702
7.5	0.55904	6.74615	0.46243
8.0	0.63912	6.21192	0.43127
8.5	0.69589	5.75718	0.40655
9.0	0.69632	5.4983	0.40777
9.5	0.72733	5.2199	0.39696
10.0	0.7261	5.00644	0.39904
10.5	0.77903	4.73629	0.3813
11.0	0.82524	4.48329	0.36541
11.5	0.81538	4.32244	0.37313
12.0	0.87083	4.1125	0.35711
12.5	0.89698	3.93998	0.3524
13.0	0.91512	3.79542	0.35263
13.5	0.7575	3.67322	0.38601
14.0	0.96742	3.54585	0.35424
14.5	0.99526	3.40041	0.34573
15.0	-0.53363	3.35038	0.48923

Slow Relaxation (SR) of **10** under zero dc field			
T / K	χ_1	χ_2	α
2.0	1.02603	24.55034	0.60133
3.0	1.40665	14.80014	0.49578
4.0	1.20051	10.84826	0.46415

5.0	0.92949	8.92852	0.47279
6.0	0.6803	7.85349	0.50212
7.0	0.5395	7.1925	0.51513
8.0	0.53743	6.31549	0.48481
9.0	0.5889	5.5199	0.42348
10.0	0.60959	4.92486	0.3609
11.0	0.70566	4.38848	0.27274
12.0	0.67455	4.0689	0.25345
13.0	0.7855	3.71896	0.20377
14.0	0.96184	3.46094	0.16598
15.0	1.27769	3.25542	0.15567
16.0	-1.87E12	3.06538	0.30051

[a] Fitting function

y = 0.5*(χ_1-χ_2)/tan((1-α)*1.5707)+sqrt((x-χ_1)*(χ_2-x)+0.25*(χ_2-χ_1)^2/(tan((1-α)*1.5707))^2)

Table S6 The parameters obtained from cole-cole plots using the Debye model for **4** and **10** under the optimum fields.

Slow Relaxation (SR) for **4** under 1000 Oe dc field			
T / K	χ_1	χ_2	α
2.0	0.67331	35.4339	0.45752
2.5	0.68426	33.43528	0.45517
3.0	0.83783	28.52702	0.42632
3.5	0.88846	26.08857	0.41932
4.0	0.92439	23.86918	0.41466
4.5	0.94648	22.03251	0.41207
5.0	1.02825	19.80397	0.3941
5.5	1.11221	17.95741	0.37458
6.0	1.08692	17.08672	0.38226
6.5	1.13335	15.85788	0.37219
7.0	1.09146	15.10355	0.38287
7.5	1.20611	13.85481	0.35732
8.0	1.26088	12.97506	0.3468
8.5	1.29464	12.14359	0.34019
9.0	1.37495	11.51352	0.3282
9.5	1.43448	10.87757	0.32023

10.0	1.50493	10.36108	0.31303
10.5	1.5922	9.80681	0.30212
11.0	1.73114	9.33316	0.28508
11.5	1.784353	8.93281	0.28549
12.0	1.83933	8.58541	0.28608
12.5	2.00677	8.22882	0.27041
13.0	2.01233	7.90978	0.27677
13.5	2.20024	7.63366	0.26398
14.0	2.54422	7.32923	0.23111
14.5	2.5251	7.09437	0.24595
15.0	3.37937	6.77922	0.13942

Slow Relaxation (SR) for **10** under 1500 Oe dc field			
T / K	χ_1	χ_2	α
2.0	0.3565	33.91192	0.4452
3.0	0.54779	25.17702	0.38053
4.0	0.68871	20.50952	0.33207
5.0	0.79672	17.16906	0.28847
6.0	0.86132	14.66936	0.25185
7.0	0.88806	12.79767	0.2232
8.0	0.88483	11.33783	0.19984
9.0	0.88097	10.0948	0.17233
10.0	0.8354	9.11519	0.15678
11.0	0.76803	8.34276	0.15262
12.0	0.86375	7.66053	0.13754
13.0	1.06489	7.08693	0.13156
14.0	1.57713	6.59291	0.11701
15.0	0.89585	6.16275	0.15803
16.0	-0.66448	5.78634	0.19119

[a] Fitting function

y = 0.5*(χ_1-χ_2)/tan((1-α)*1.5707)+sqrt((x-χ_1)*(χ_2-x)+0.25*(χ_2-χ_1)^2/(tan((1-α)*1.5707))^2)

Table S7 Dy-SMMs based on the different 8-hydroxyquinoline Schiff base ligands and β-diketonate coligands (H_{dc} = 0 Oe).

Dy-SMMs	β-diketonates	Cryst syst	Space group	U_{eff} / K	τ_0 / s	α	References
$[Dy_4(acac)_4L_6(\mu_3\text{-}OH)_2]$	acac	Orthorhombic	*Pbcn*	48(FR) 121(SR)	2.2×10^{-7} 2.8×10^{-8}	0.29–0.55 0.069–0.21	[25(b)]
$[Dy_4(dbm)_4L_6(\mu_3\text{-}OH)_2]$	dbm	Monoclinic	$P2_1/c$	56	2.64×10^{-7}	0.39–0.48	[25(c)]
$[Dy_4(acac)_4L_6(\mu_3\text{-}OH)_2]\cdot4CH_3CN$	acac	Monoclinic	$P2_1/c$	37.49(FR) 89.89(SR)	7.73×10^{-6} 5.56×10^{-7}	0.16–0.60	this work
$[Dy_4(dbm)_4L_6(\mu_3\text{-}OH)_2]\cdot3CH_3CN$	dbm	Triclinic	$P\bar{1}$	93.23	3.38×10^{-7}	0.35–0.56	
$[Dy_2(tfac)_4L_2]$	tfac	Monoclinic	$C2/c$	9.61	4.76×10^{-6}	0.04–0.11	
$[Dy_2(TTA)_4L_2]$	TTA	Triclinic	$P\bar{1}$	54.81	3.74×10^{-7}	0.11–0.23	[9(b)]
$[Dy_2(dbm)_4L_2]\cdot2CH_3CN\cdot0.5H_2O$	dbm	Triclinic	$P\bar{1}$	30.98	4.20×10^{-6}	0.20–0.29	
$[Dy_2(hfac)_4L_2]$	hfac	Monoclinic	$P2_1/n$	6.77	9.12×10^{-6}	0.25–0.29	
$[Dy_2(tfac)_4L_2]$	tfac	Monoclinic	$P2_1$	19.83	7.62×10^{-8}	0.34–0.40	[25(a)]
$[Dy_2(bfac)_4L_2]\cdot C_7H_{16}$	bfac	Triclinic	$P\bar{1}$	25.65	1.64×10^{-6}	0.27–0.32	

(tfac = trifluoroacetylacetonate, TTA = 2-thenoyltrifluoroacetone, hfac = hexafluoroacetylacetonate, bfac = benzoyltrifluoroacetone, dbm = dibenzoylmethane, acac = acetylacetonate.)

Section S5 Supplementary Figures

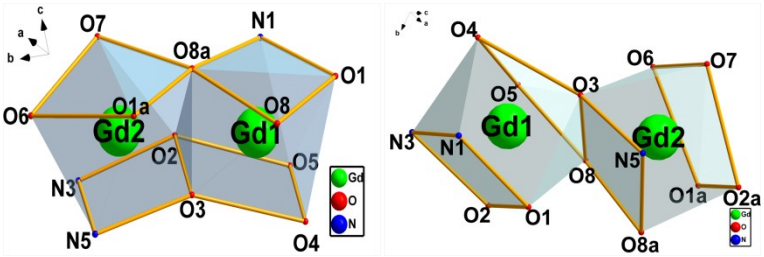

Fig. S1 The coordination polyhedrons for the adjacent Gd^{III} ions in complex **2** and **8** (left and right).

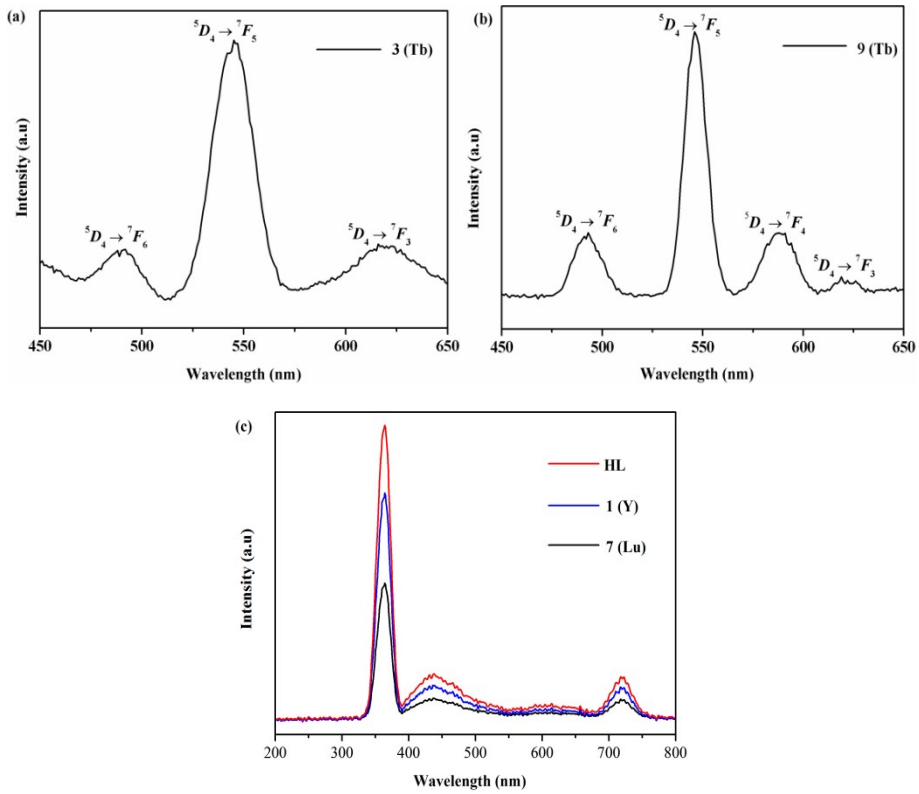

Fig. S5 The luminescence spectra of complex **3** (a), **9** (b), and complex **1**, **7** and HL (c) in methanol solution.

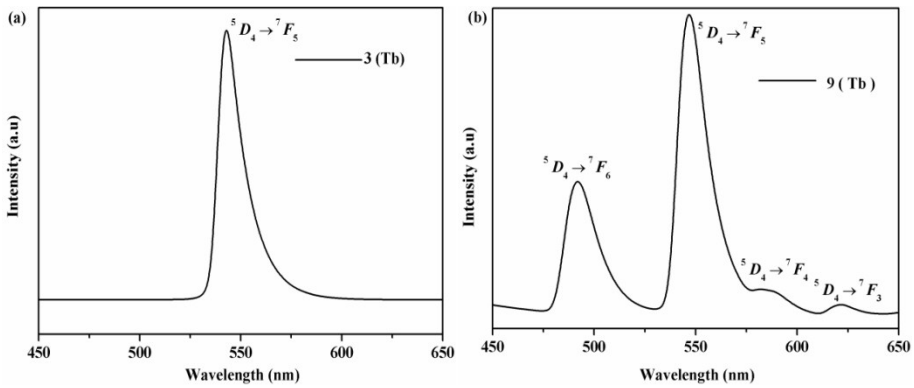

Fig. S6 The luminescence spectra of complex **3** (a) and **9** (b) in the solid state.

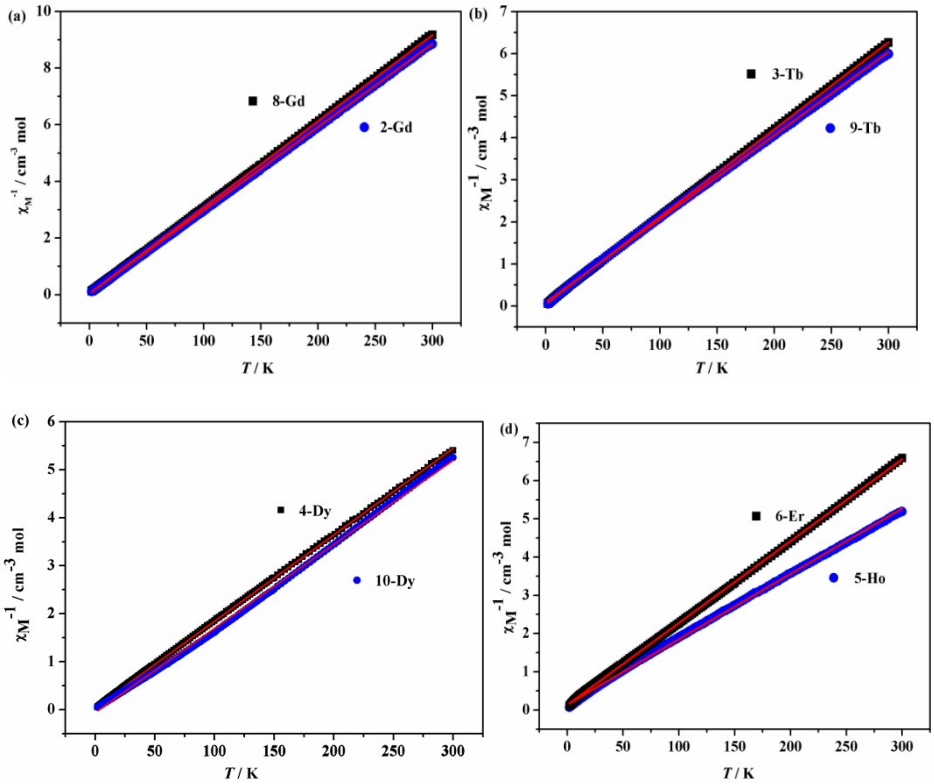

Fig. S7 Plots of χ_M^{-1} vs T for Gd_4, Dy_4, Tb_4, Ho_4 and Er_4 (a, b, c, d). The solid line was generated from the best fit by the Curie-Weiss expression.

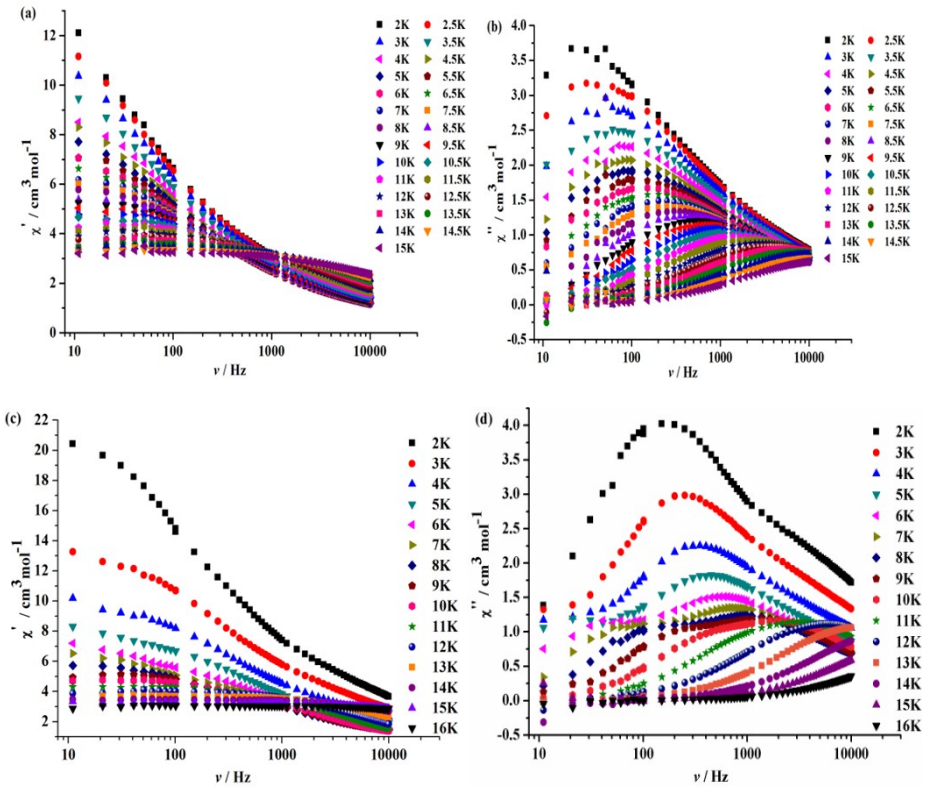

Fig. S8 The frequency dependence of χ′ and χ″ for **4** (a and b) and **10** (c and d) under zero-dc field.

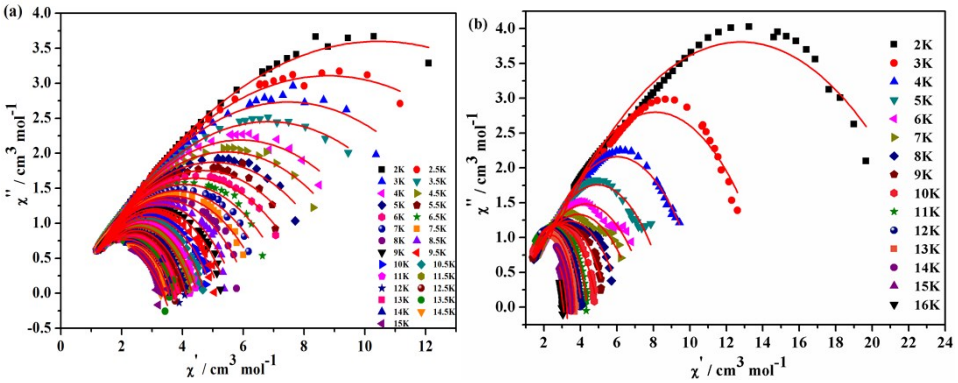

Fig.S9 Cole-cole plots for **4** and **10** (a and b) measured in zero dc field. The red solid lines represent the best fit with the generalized Debye model.

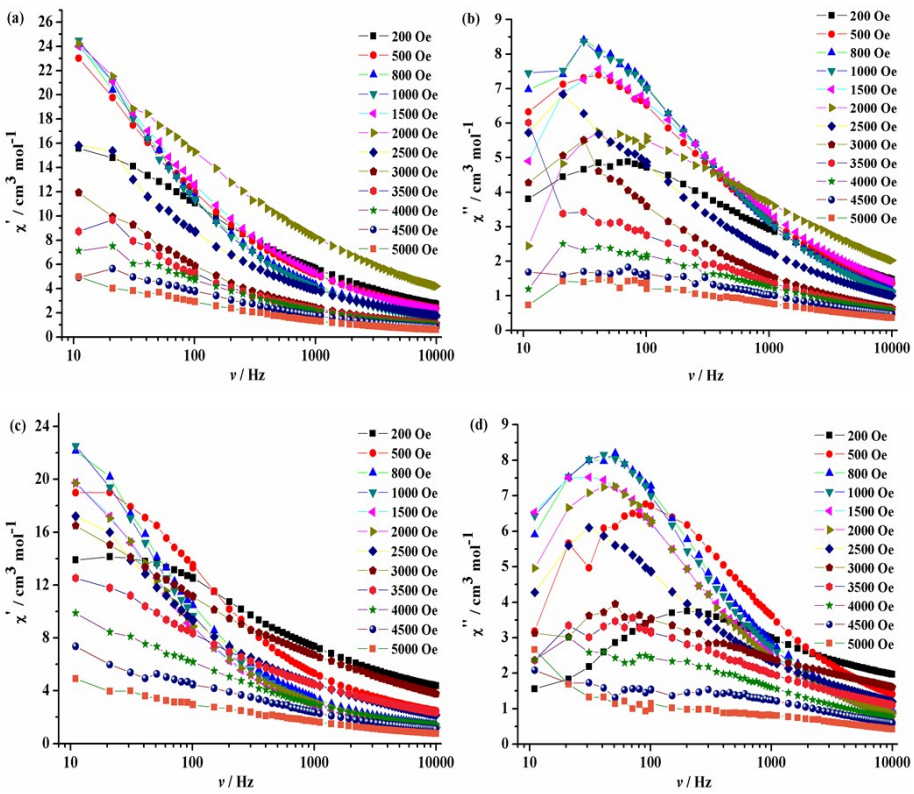

Fig. S10 The frequency dependency of the ac susceptibility was measured on powder samples **4** (a, b) and **10** (c, d) in the applied field from 200 to 5000 Oe at 2 K.

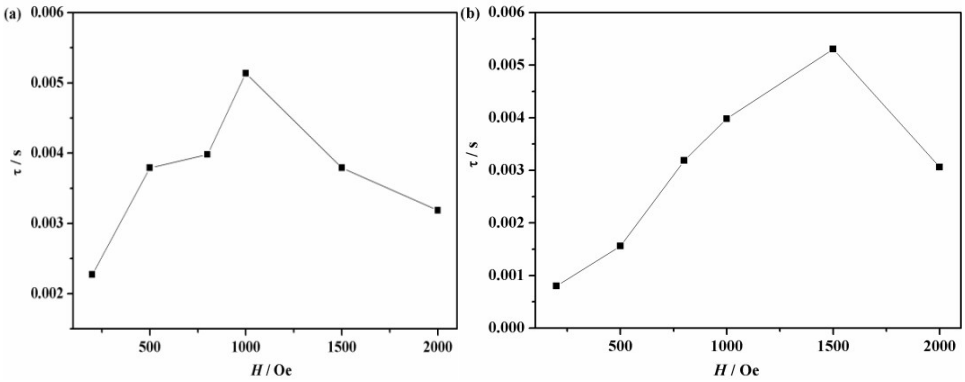

Fig. S11 The τ versus H plots for complexes **4** and **10** (a and b) under the applied dc field.

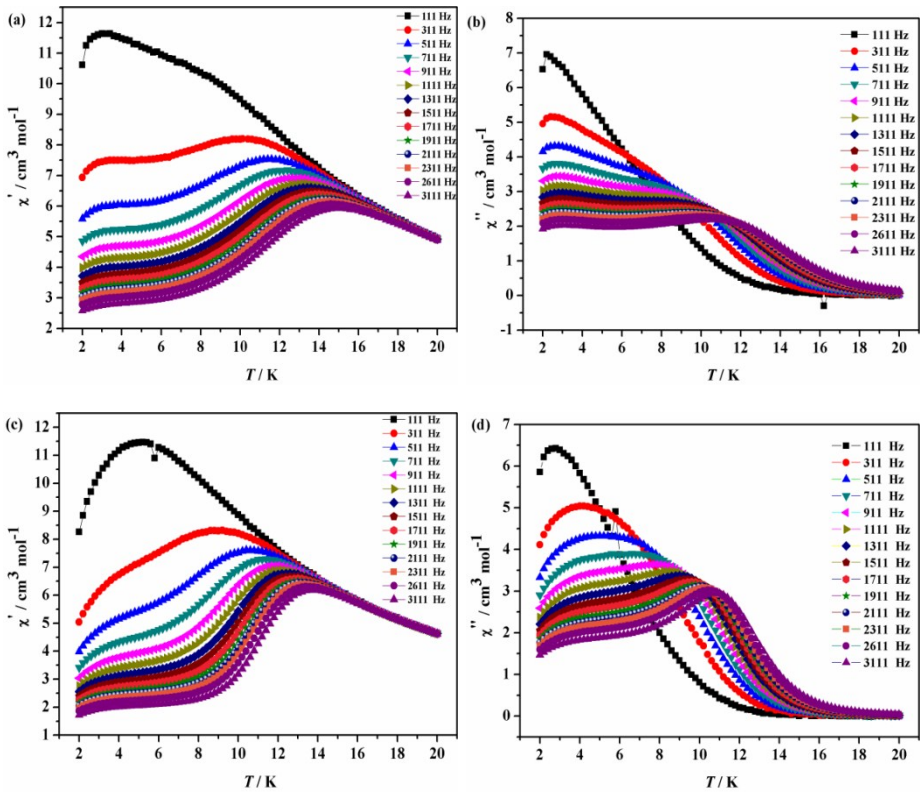

Fig. S12 The temperature dependence of χ′ and χ″ for **4** (a and b) under a 1000 Oe dc field and **10** (c and d) under a 1500 Oe dc field.

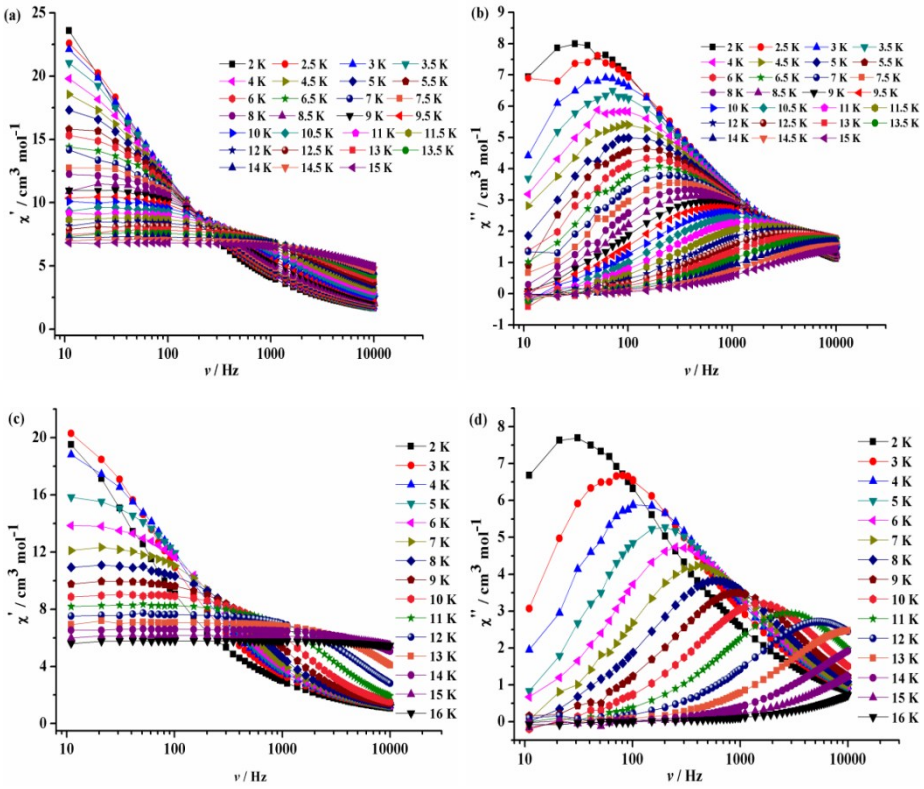

Fig. S13 The frequency dependence of χ′ and χ″ for **4** (a and b) under a 1000 Oe dc field and **10** (c

and d) under a 1500 Oe dc field.

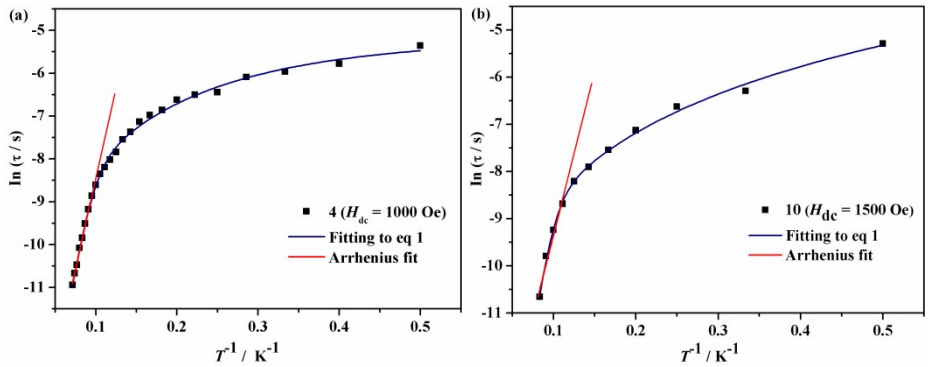

Fig. S14 The ln (τ) versus T^{-1} plots for **4** (a) under a 1000 Oe dc field and **10** (b) under a 1500 Oe dc field; the red solid line is best fitted with the Arrhenius law, the navy solid line is best fitted with the eq 1.

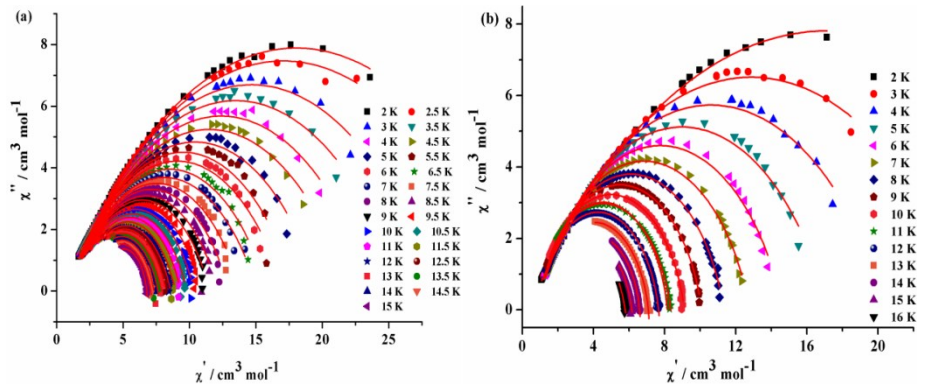

Fig. S15 Cole-cole plots for **4** (a) under a 1000 Oe dc field and **10** (b) under a 1500 Oe dc field. The red solid lines represent the best fit with the generalized Debye model.